

3D-Aware Video Generation

Sherwin Bahmani¹ Jeong Joon Park² Despoina Paschalidou² Hao Tang¹
 Gordon Wetzstein² Leonidas Guibas² Luc Van Gool^{1,3} Radu Timofte^{1,4}

¹ETH Zürich ²Stanford University ³KU Leuven ⁴University of Würzburg

Abstract

Generative models have emerged as an essential building block for many image synthesis and editing tasks. Recent advances in this field have also enabled high-quality 3D or video content to be generated that exhibits either multi-view or temporal consistency. With our work, we explore 4D generative adversarial networks (GANs) that learn unconditional generation of 3D-aware videos. By combining neural implicit representations with time-aware discriminator, we develop a GAN framework that synthesizes 3D video supervised only with monocular videos. We show that our method learns a rich embedding of decomposable 3D structures and motions that enables new visual effects of spatio-temporal renderings while producing imagery with quality comparable to that of existing 3D or video GANs.



Figure 1: 3D-Aware video generation. We show multiple frames and viewpoints of a 3D video, generated using our model trained on the FaceForensics dataset [83]. Our 4D GAN generates 3D content of high quality while permitting control of time and camera extrinsics. Video results can be viewed on our website: <https://sherwinbahmani.github.io/3dvidgen>

1 Introduction

Recent advances in generative adversarial networks (GANs) [25] have led to artificial synthesis of photorealistic images [44, 45, 43]. These methods have been extended to enable unconditional generation of high-quality videos [11, 116] and multi-view-consistent 3D scenes [28, 9, 72]. However, despite important applications in visual effects, computer vision, and other fields, no generative model has been demonstrated that is successful in synthesizing 3D videos to date.

We propose the first 4D GAN that learns to generate multi-view-consistent video data from single-view videos. For this purpose, we develop a 3D-aware video generator to synthesize 3D content that is animated with learned motion priors, and permits viewpoint manipulations. Two key elements of our framework are a time-conditioned 4D generator that leverages emerging neural implicit scene representations [74, 61, 63] and a time-aware video discriminator. Our generator takes as input two latent code vectors for 3D identity and motion, respectively, and it outputs a 4D neural fields that can

be queried continuously at any spatio-temporal $xyzt$ coordinate. The generated 4D fields can be used to render realistic video frames from arbitrary camera viewpoints. To train the 4D GAN, we use a discriminator that takes two randomly sampled video frames from the generator (or from real videos) along with their time differences to score the realism of the motions. Our model is trained with an adversarial loss where the generator is encouraged, by the discriminator, to render realistic videos across all sampled camera viewpoints.

We evaluate the effectiveness of our approach on challenging, unstructured video datasets. We show that the trained 4D GAN is able to synthesize plausible videos that allows viewpoint changes, whose visual and motion qualities are competitive against the state-of-the-art 2D video GANs’ outputs. Lastly, to encourage future research on 4D GAN, we justify our design decisions via ablation studies.

2 Related Work

In this section, we discuss the most relevant literature on image and video synthesis as well as neural implicit representations in the context of 2D and 3D content generation.

GAN-based Image Synthesis Generative Adversarial Networks (GANs) [25] have demonstrated impressive results on multiple synthesis tasks such as image generation [7, 16, 35, 44, 45], image editing [109, 89, 3, 53, 107] and image-to-image translation [38, 124, 16, 97, 98]. To allow for increased controllability, during the image synthesis process, several recent works have proposed to disentangle the underlying factors of variation [81, 13, 121, 47, 90] or rely on pre-defined templates [99, 100]. However, since most of these methods operate on 2D images, they tend lack physically-sound control in terms of viewpoint manipulation. In this work, we advocate modelling both the image and the video generation process in 3D in order to ensure controllable generations.

Neural Implicit Representations Among multiple 3D representations proposed for generating 3D content, Neural Implicit Representation (NIR) [61, 74, 14, 62] stand out as a continuous, efficient, and differentiable representation. Among the most widely used NIR works are Neural Radiance Fields (NeRFs) [63] that combine an implicit neural network with volumetric rendering to enforce 3D consistency while performing the novel view synthesis task. NIRs have been extensively adopted for multiple tasks in 3D vision including 3D reconstruction of objects [61, 74, 14, 62, 24, 71, 27, 86, 4, 93] and scenes [39, 15, 77, 8, 92], novel-view synthesis of static [63, 5, 6, 23, 39, 54, 52, 96, 78, 58, 71, 87] and dynamic [56, 48, 79, 75, 112, 117, 76, 103, 101] environments, inverse graphics [70, 115, 50] as well as for representing videos [11, 116]. In this work, we employ a generative variant of NeRF [28] for explicitly modelling the image formation process and combine it with a time-aware discriminator to learn a generative model of videos from unstructured videos.

Closely related to our work are recent approaches that control the motion and pose of the reconstructed scenes [51, 12, 55, 119, 82]. These methods focus on transferring or controlling the motion of their target objects instead of automatically generating plausible motions. They often use networks overfitted to a single reconstructed scene [12, 119] or rely on pre-defined templates of human faces or bodies [55, 82]. In our work, we build a 4D generative model that can automatically generate diverse 3D content along with its plausible motion without using any pre-defined templates.

3D-Aware Image Generations Many recent models investigate how 3D representations can be incorporated in generative settings for improving the image quality [73, 65] and increasing the controllability over various aspects of the image formation process [21, 10, 30, 32, 31, 49, 57, 66, 67, 88, 28, 19, 29, 59, 68, 123]. Towards this goal, several works [32, 66, 67] proposed to train 3D-aware GANs from a set of *unstructured single-view* images using voxel-based feature representations. However, these works suffer from either the low-resolution nature of voxels or the inconsistent view-controls because of their use of pseudo-3D structures that rely on non-physically-based 2D-3D conversions. More recent approaches propose generative models using MLP-based radiance fields. These methods use volume rendering to obtain images from the 3D fields to model single [88, 10] or multiple [69] objects. Similarly, [123, 10, 19] explored the idea of combining NeRF with GANs for designing 3D-aware image generators. More recently, StyleSDF [72] and StyleNeRF [28] proposed to combine an MLP-based volume renderer with a style-based generator [45] to produce high-resolution 3D-aware images. [18] explored learning a generative radiance field on 2D manifolds and [9] introduced a 3D-aware architecture that exploits both implicit and explicit representations.

In contrast to this line of research that focuses primarily on 3D-aware image generation, we are interested in *3D-aware video generation*. In particular, we build on top of StyleNeRF [28] to allow control both on the 3D camera pose as well as on the time during the video synthesis. To the best of our knowledge, this is the first work towards 3D-aware video generation trained from unstructured 2D data.

GAN-based Video Synthesis Inspired by the success of GANs and adversarial training on photorealistic image generation, researchers shifted their attention to various video synthesis tasks [84, 104, 1, 17, 118, 40, 2, 85, 26, 34, 64, 102, 20, 114, 37, 116, 95]. Several recent works pose the video synthesis as an autoregressive video prediction task and seek to generate discrete future frames conditioned on the previous using either recurrent [41, 106] or attention-based [80, 111, 114] models. Other works on video generation [84, 104, 2, 85] tried to disentangle the motion from the image generation during the video synthesis process. While this paradigm has been widely adopted, these approaches typically struggle to generate realistic videos. To facilitate generating high-quality frames, [102, 20] propose to employ a pre-trained image generator of [45]. Closely related to our method are the recent and concurrent work of DIGAN [116] and StlyeGAN-V [95] that generate videos at continuous time step, without conditioning on previous frames. DIGAN [116] employs an NIR-based image generator [94] for learning continuous video synthesis and introduces two discriminators: the first discriminates the realism of each frame and the second operates on image pairs and seeks to determine the realism of the motion. Similarly, StyleGAN-V [95] employs a style-based GAN [45] and a single discriminator that operates on sparsely sampled frames. In contrast to [116, 95] that do not consider images as projections of the 3D world, we focus on *3D-aware video generation*. In particular, we build our model on top of StyleNeRF [28] and DIGAN [116] and demonstrate its ability to render high quality videos from diverse viewpoint angles. Note that this task is not possible for prior works that do not explicitly model the image formation process in 3D.

3 Method

The two main components of our 4D GAN framework are a time-conditioned neural scene generator and a time-aware discriminator. Our generator networks take as input two independent noise vectors, \mathbf{m} and \mathbf{z} , that respectively modulate the motion and the content of the 4D fields. To render an image at a specific time step t , we sample the camera extrinsics according to dataset-dependent distribution and conduct volume rendering through the time-conditioned radiance and density fields. Our time-aware discriminator measures the realism of a pair of frames, given their time difference, to promote plausible 3D video generation. The overview of our pipeline can be found in Fig. 2.

3.1 Time-Conditioned Implicit Fields

We build on top of existing coordinate-based neural generators [28, 72, 9] to model continuous implicit fields using a Multi-layer Perceptron (MLP) that outputs a density $\sigma(\mathbf{x}, t; \mathbf{z}, \mathbf{m})$ and appearance feature $\mathbf{f}(\mathbf{x}, t, \mathbf{d}; \mathbf{z}, \mathbf{m})$ for a given spatio-temporal query (\mathbf{x}, t) , and view direction \mathbf{d} . Here, \mathbf{z} and \mathbf{m} are 3D content and motion latent vectors, respectively. While it is possible to factor in both motion and content into a single vector, we find that using separate vectors boosts generation quality and promotes an useful decomposition of motion and content.

We process a motion latent vector \mathbf{m} sampled from a unit sphere with an MLP conditioned on time step $t \in [0, 1]$, to obtain a final motion vector \mathbf{n} :

$$\mathbf{n}(\mathbf{m}, t) = \psi^3 \circ \psi^2 \circ (t \cdot (\psi^1 \circ \mathbf{m})), \quad (1)$$

where ψ^i is a fully connected layer. Leaky ReLU activation is applied between the layers. Note that our use of continuous time variable t allows rendering the video at an arbitrary frame rate, unlike autoregressive models that can only sample discrete time steps.

The resulting motion vector $\mathbf{n}(\mathbf{m}, t)$ is then used to control the output of the generator MLP $g_{\mathbf{w}}(\mathbf{x}, \mathbf{n})$ along with the modulation parameters $\mathbf{w}(\mathbf{z})$ computed from the 3D content vector \mathbf{z} :

$$g_{\mathbf{w}}(\mathbf{x}, \mathbf{n}) = \phi_{\mathbf{w}}^k \circ \phi_{\mathbf{w}}^{k-1} \circ \dots \circ \phi_{\mathbf{w}}^2 \circ (\mathbf{n}(\mathbf{m}, t) + \phi_{\mathbf{w}}^1 \circ \gamma(\mathbf{x})), \quad (2)$$

where $\phi_{\mathbf{w}}^i$ is a fully connected layer (with Leaky ReLU activations between the layers) whose weights are modulated by the style vector \mathbf{w} , following the style-based generation techniques [28, 45]. The

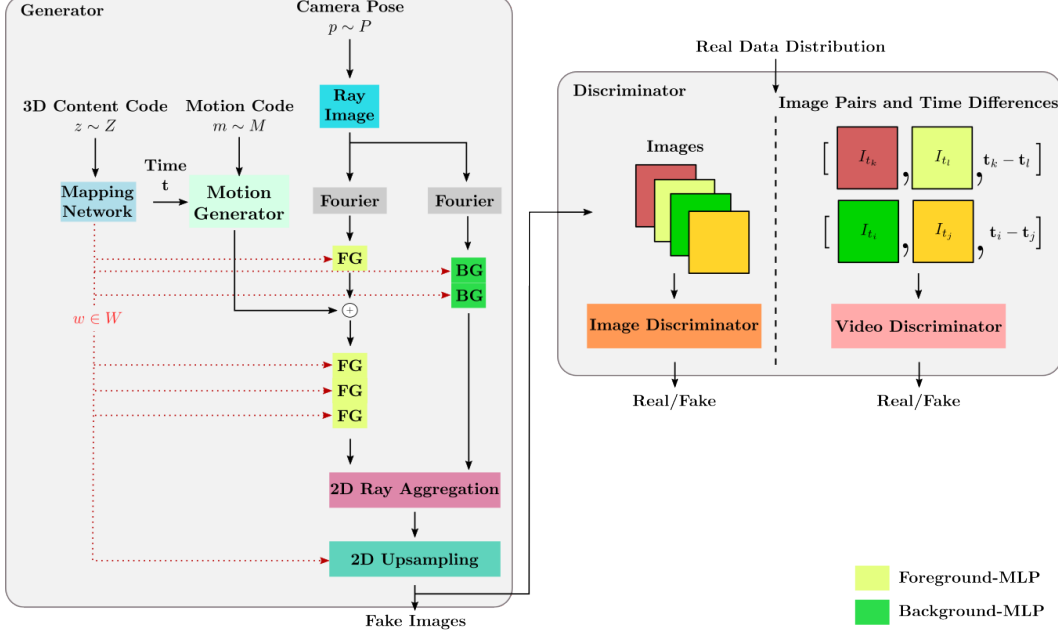


Figure 2: Model architecture. The generator (left) takes 3D content and motion codes and the query camera view to render an RGB image. Given a camera pose, we construct a ray image, from which we sample xyz positions along the rays to be passed to the fourier feature layer. The content code is transformed into w and modulate the intermediate features of MLP layers. The motion code, along with the time query t , is processed with the motion generator and added to the generator branch. The video discriminator takes two random frames from a video and their time difference and outputs real/fake prediction. The image discriminator takes individual frames and outputs real/fake label.

style vector is produced with a mapping MLP network: $w = \text{MLP}_{\text{content}}(z)$, where z is sampled from the surface of unit sphere. $\gamma(x)$ is a positional encoding vector of a spatial query x that induces sharper appearances, following [63]. We omit positional encoding on the time step t , as the empirical results did not improve (see Sec. 4.3).

The density value at x is then computed by passing the feature $g_w(x, n)$ to a two layer MLP ϕ_σ :

$$\sigma(x, t; z, m) = \phi_\sigma \circ g_w(z)(x, n(t, m)) \quad (3)$$

Image Rendering To render an image from a virtual camera with pose p , we compute an appearance feature for a ray $r(l) = o + ld$ going through each pixel that emanates from the camera focus o towards the direction d . Specifically, we approximate the volume rendering process [63] with discrete point sampling along the rays and process the aggregated ray features with an MLP, denoted h_w , conditioned on the view direction d :

$$f(r, t, d; z, m) = h_w \circ \left[\gamma(d), \int_{l_i}^{l_f} T(l) \sigma(r(l), t) g_w(r(l), n) dl \right], \quad (4)$$

$$\text{where } T(l) = \exp\left(-\int_{l_i}^l \sigma(r(s), t) ds\right).$$

The volume rendering of Eq. 4 involves millions of MLP queries and thus becomes quickly intractable with high resolution images. To reduce the computational overhead, we adopt the 2D upsampling CNN of StyleNeRF [28] to convert the low-resolution volume rendering results of f into a high-resolution RGB image \mathcal{I} :

$$\mathcal{I}_p(t; z, m) = \text{CNN}_{\text{up}}(f(\mathcal{R}_p, t, d; z, m)), \quad (5)$$

where \mathcal{R}_p denotes an image composed of rays from camera pose p , with slight abuse of notation.

Background and Foreground Networks A typical video is composed of static background and moving foreground. Intuitively, it would be ineffective to model both foreground and background using one network and motion code. We follow the inverse sphere parameterization of [120] to model the background with a second MLP network of g_w that is modulated only with the content vector.

3.2 Training

We train our 4D generator via adversarial loss, leveraging time-aware discriminators from the video GAN literature. The key idea of our training is to encourage the generator to render realistic video frames for all sampled viewpoints and time steps, by scoring their realism with the discriminators.

Time-Aware Discriminator Unlike autoregressive generators, our continuous 4D generator can render frame at an arbitrary time step without knowing the 'past' frames. This feature allows using efficient time-aware discriminators [95, 116] that only look at sparsely sampled frames as oppose to entire video that often requires expensive 3D convolutions to process. We adopt the 2D CNN discriminator D_{time} of DIGAN [116] to score the realism of the generated motion from two sampled frames. Specifically, we render a pair of frames $\mathcal{I}_p(t_1; \mathbf{z}, \mathbf{m})$ and $\mathcal{I}_p(t_2; \mathbf{z}, \mathbf{m})$ from the same 3D scene and camera pose. The input to the discriminator D_{time} is a concatenation of the two RGB frames along with the time difference between the frames expanded to the image resolution $\mathcal{I}_{\text{repeat}}(t_2 - t_1)$:

$$D_{\text{time}} : [\mathcal{I}_p(t_1; \mathbf{z}, \mathbf{m}), \mathcal{I}_p(t_2; \mathbf{z}, \mathbf{m}), \mathcal{I}_{\text{repeat}}(t_2 - t_1)] \rightarrow \mathbb{R}, \quad \text{where } t_2 > t_1. \quad (6)$$

For real videos, we similarly pass a random pair of frames along with their time difference to D_{time} .

Single Image Discriminator In theory, the time-aware discriminator D_{time} should be able to simultaneously measure the realism of the motion of the input pair and that of individual frames. In practice, however, we find that training a separate discriminator that specializes in single frame discrimination improves quality (see Sec. 4.3). We therefore adopt another discriminator D_{image} that scores realism of individual images: $D_{\text{time}} : \mathcal{I}_p(t; \mathbf{z}, \mathbf{m}) \rightarrow \mathbb{R}$. Following 3D GAN approaches [28, 72, 9], we use StyleGAN2 [45] discriminator architecture without modifications.

Loss Function The overall objectives of our training include the adversarial losses from the two discriminators along with the R1 [60] and NeRF-Path regularizations [28]:

$$\mathcal{L}(D, G) = \mathcal{L}_{\text{adv}}(D_{\text{time}}, G) + \mathcal{L}_{\text{adv}}(D_{\text{image}}, G) + \lambda_1 \mathcal{L}_{\text{R1}}(D_{\text{time}}, D_{\text{image}}) + \lambda_2 \mathcal{L}_{\text{NeRF-path}}(G), \quad (7)$$

where G denotes the entire image generator machinery in Eq. 5, and λ 's are balancing parameters. For computing the adversarial losses we use the non-saturating objective. Note that our networks are trained end-to-end without the progressive growing strategy. Refer to the supplementary materials for more details on the training procedures.

Training on Image and Video Datasets The 3D structure of our generator emerges without 3D supervision by enforcing adversarial loss from sampled camera views. Thus, it is crucial that our video dataset features a diverse set of view angles. However, we notice that many of the popular video GAN datasets feature narrow range of viewpoints (e.g., FaceForensics). To address this issue, we seek to leverage existing 2D image datasets that are typically greater in quantity and diversity.

We explore two options: (1) We pre-train our generator model G on an image dataset and fine-tune it on a video dataset. During pre-training, we ignore the temporal components and sample the 3D content only. Such training can be done seamlessly by simply setting the motion vector $\mathbf{n}(\mathbf{m}, t)$ of Eq. 2 to be zero. After pre-training, we unfreeze the temporal components and minimize the whole objective (Eq. 7) on a video dataset. (2) We train our generator on image and video datasets simultaneously. The training could be done in an alternating fashion, switching between samples from the two datasets. Refer to supplementary for more details and analysis of these two options.

4 Experiments

We conduct experiments to demonstrate the effectiveness of our approach in generating 3D-aware videos, focusing on the new visual effects it enables and the quality of generated imagery. To benefit future research in 4D generative model, we conduct extensive ablation studies on the design components of our model.

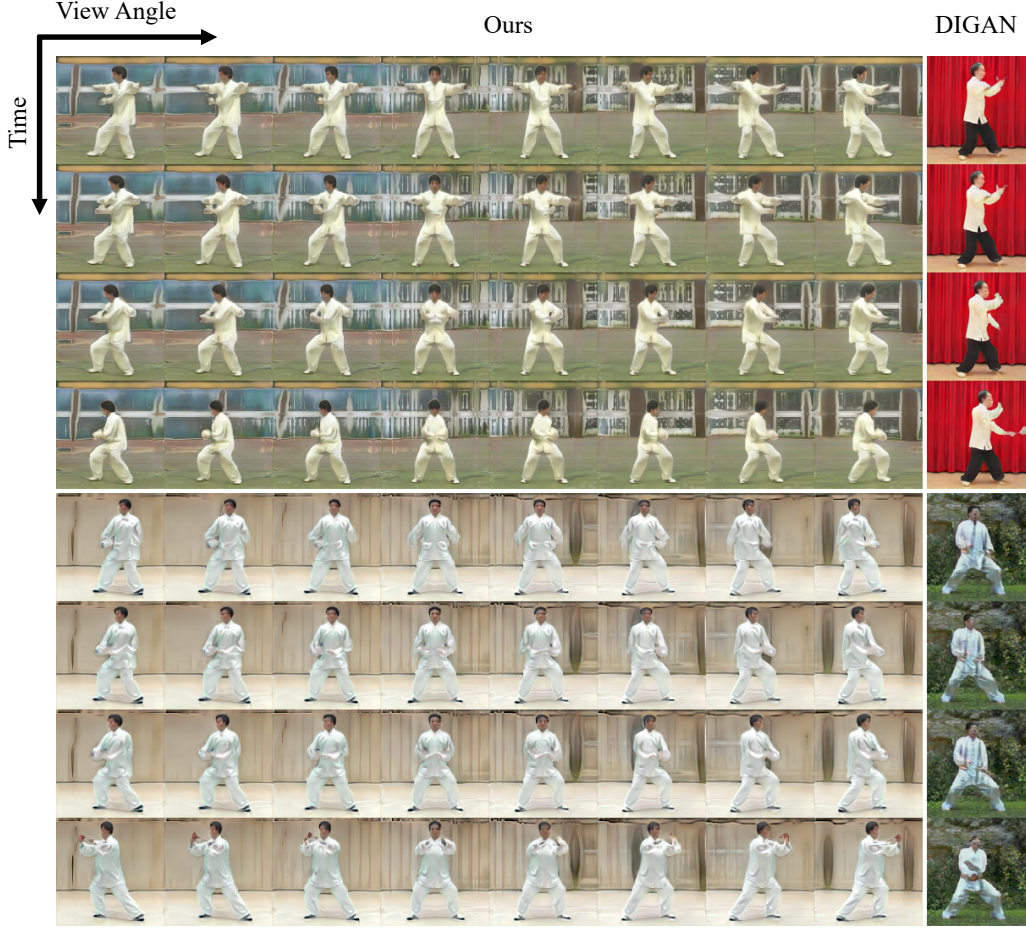


Figure 3: Qualitative results on TaiChi dataset. We visualize the spatio-temporal renderings of two scenes sampled from our 4D GAN, where the horizontal axis indicates change of view angles while the vertical axis indicates progress of time. The rightmost column shows two videos sampled from DIGAN [116] that can only be viewed from a fixed camera angle. Our method extends DIGAN in the spatial dimension while producing frames of comparable quality.

4.1 Experiment Setups

Datasets We evaluate our approach on publicly available, unstructured video datasets: FaceForensics [83], MEAD [108], and TaiChi [91] datasets. FaceForensics dataset contains 1004 videos of human faces sourced from YouTube, from which select 704 for training. While the dataset containing in-the-wild videos makes it a great testbed for synthesis algorithms, many of its videos are captured from frontal views with limited view diversity. On the other hand, MEAD dataset contains a large set of short videos capturing faces from discrete 7 angles, from which we randomly subsample 10,000. We ignore the identity correspondences of the videos and treat them as independent unstructured videos. The TaiChi dataset presents a challenging setup, containing 2942 in-the-wild videos of highly diverse TaiChi performances sourced from the internet. Following DIGAN [116], we use one every four frames to make the motion more dynamic. Finally, we run additional experiments on SkyTimelapse dataset [113], where the details and results can be found in the supplementary.

Metrics Following the previous 2D video generation works, we use Frechet Video Distance (FVD) [105] as our main metric for measuring realism of the generated 16-frame motion sequences. We follow the FVD evaluation protocol and code of StyleGAN-V [95] that alleviate the inconsistency issues of the original FVD evaluation code [105]. To provide common metric to 2D and 3D-aware image generation methods that cannot synthesize videos, we use the popular Frechet Image Distance (FID) [33] as an auxiliary metric for FaceForensics dataset. The individual frames for FID scores are



Figure 4: Qualitative results on FaceForensics Dataset. The first 6 columns visualize two 4D fields sampled from of our model trained on FaceForensics rendered from various spatio-temporal snapshots. Note the high quality visuals and motions across diverse viewpoints. The last three columns show the video samples of MoCoGAN-HD [102], DIGAN [116], and StyleGAN-V [95], in that order.

randomly selected from all generated video frames. For each method, we choose a model checkpoint with the lowest FVD score (or FID scores if not applicable).

4.2 Main Results

3D-Aware Videos Figures 1, 3, 4, and 5 show snapshots of sampled 4D scenes rendered from various time steps and camera angles across the datasets. These results demonstrate our model’s capability to learn a distribution of 3D-aware videos that permit spatio-temporal control.

Comparisons We conduct both qualitative and quantitative comparisons against the strongest video GAN baselines on the three datasets. For each method, we use video length of 16 frames and use image resolution of 256^2 for FaceForensics and MEAD, and 128^2 for TaiChi dataset.

FaceForensics is one of the most widely used dataset in the video generation literature, and thus we measure the scores across a wide range of methods, including: 2D image [45] and video generation works [116, 95, 104, 102, 114], and a 3D generation method [28]. The qualitative results in Fig. 4 show our model’s ability to generate 4D visual effects, displaying the spatiotemporal renderings and the physically-based zoom-in effects. The quantitative results in Table 1 confirm that our generated imagery are of competitive quality against the strongest 2D and 3D baselines despite that our approach models additional dimensions. Note that the metrics for the 2D image and video methods are copied from the reports of [95]. We train StyleNeRF [28] on FaceForensics from scratch.

Fig. 3 presents sampled scenes from our TaiChi-trained model with varying time and viewpoints, showcasing our 4D learning on a challenging setup with complex motions and backgrounds. When compared with one of the latest 2D video generation method, DIGAN [116] (right-most column), our method synthesizes frames with competitive visual fidelity while introducing another degree of freedom. Quantitatively, our FVD score was 158.3 compared to 151.7 of DIGAN [116], where we use the provided pre-trained model to recompute their score following the protocol used in [95].

The experiment on the MEAD dataset is noteworthy, as the dataset contains videos taken from a wide range of viewpoints. We hypothesize that, for the 2D-based methods, a significant amount of expressive power will be used for redundantly modeling the diverse views in 2D, while the 3D approach would only need to learn a shared representation across views. The results, shown in Fig. 5, indeed suggest higher visual quality for our 4D approach, while allowing rendering from 7 different viewpoints. The numerical results support our observation – FVD of our generated videos (55.4) is noticeably better than the FVD of StyleGAN-V [95] (109.3). Note that the pre-trained model provided by [95] was only trained on frontal faces, so we included non-frontal faces and re-trained. We omit comparing against other video methods that are already compared with [95] in their paper.

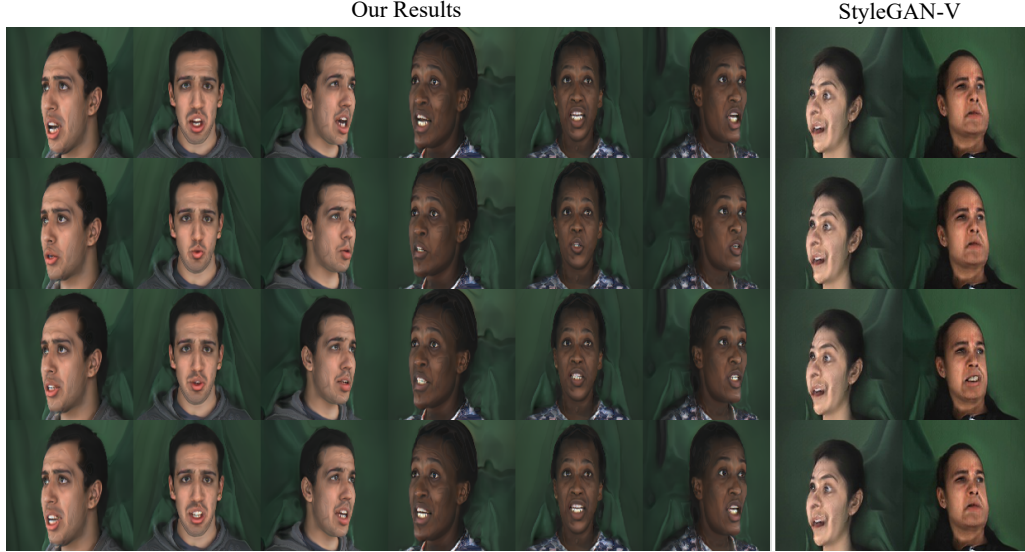


Figure 5: Results on the MEAD dataset. The first six columns show the spatio-temporal renderings of our 4D GAN, where the vertical axis indicates the progress of time. The right two columns visualize the two sample videos generated from StyleGAN-V [95]. Zoom-in to inspect details.

Type	Method	FVD	FID
2D Image	StyleGAN2 [45]	-	8.4
2D Video	VideoGPT [114]	185.9	22.7
	MoCoGAN [104]	124.7	24.0
	MoCoGAN-HD [102]	111.8	7.1
	DIGAN [116]	62.5	19.1
	StyleGAN-V [95]	47.4	9.4
3D Static	StyleNeRF [28]	-	15.3
3D Video	Ours	68.7	13.7

Table 1: Quantitative results on FaceForensics. We report FVD (\downarrow) and FID (\downarrow) for our baselines and our method at 256^2 pixel resolution.

Decomposition of Motion and Content Our method uses two independently sampled latent vectors to modulate motion and content, which makes these two components separable. Fig. 6 showcases such decomposition by applying two different motion codes to the same content code.

Supplementary Results We encourage readers to view the supplementary material for a larger set of results and watch the videos to fully appreciate our 4D content.

4.3 Ablation

We conduct ablation studies to gauge how the design choices of our algorithm affect the quality of 4D scene generations. We use TaiChi dataset, as its diverse scenes and motions help us identify the effects of each component. Table 2 summarizes the numerical results.

Background NeRF We analyze the importance of the background NeRF based on the inverse sphere parametrization of NeRF++ [120] used for capturing unbounded scenes. We observe that using the additional background NeRF is critical for the model to disentangle the dynamic and static parts in the video, leading to less motion artifacts and more static backgrounds.

Static and Dynamic Separation We forgo the use of the aforementioned inverse sphere background NeRF of [120] and instead decompose the scene with static and dynamic NeRFs, following



Figure 6: Motion and content decomposition experiment. The two rows show respective video sequences that share the same 3D content latent vector applied to different motion vectors. Note the difference in motions while the identities of the person appear unchanged.

[22]. We observe that this setup hurts the generation quality, suggesting that the background parameterization of NeRF++ [120] is critical for training a 4D generative model.

Motion Generator Here, we omit the use of a motion vector and the mapping MLP, and instead add the time value directly to the input layer of the foreground NeRF. The motion network formulation improves output quality and induces the useful decomposition of motion and 3D content.

Positional Time Encoding Our current motion mapping MLP is conditioned on the raw time value. We observe that applying the positional encoding into fourier features [63] leads to repetitive and unnatural motions even when tuning the frequencies of the fourier features. We leave applying more complicated positional encoding of time, as suggested in [95], for example, as future work.

Image Discriminator Our experiment shows that the addition of a discriminator that specializes on single-frame discrimination improves quality compared to using a time-aware discriminator alone.

Method	FVD
Ours	158.3
w/o Background NeRF	203.7
w/ Static and Dynamic Separation	207.6
w/o Motion Generator	166.3
w/ Positional Time Encoding	175.4
w/o Image Discriminator	190.9

Table 2: Ablation studies on TaiChi Dataset.

5 Limitations & Discussions

Currently, our approach implicitly decomposes the scenes into background and dynamic foreground, which is critical to the performance (see Sec. 4.3). However, modeling the entire dynamic foreground with a single latent vector limit the expressive capacity of our generative model. Learning with more number of independent latent vectors, as tried in GIRAFFE [69] or GANsformer [36], could promote modeling of multi-objected scenes with more complex motions. Furthermore, our training scheme assumes static camera and dynamic scenes, so it cannot handle videos taken from a moving camera. Modeling and generating plausible camera paths is an interesting but less explored problem. Lastly, being the first 4D GAN approach, our method models the scene motion as a purely statistical phenomenon, without explicitly considering physics, causality, semantics, and entity-to-entity interactions. These topics remain important challenges, which we continue to explore.

Potential negative Societal Impacts Our 3D video generation has potential threats of creating content for unethical purposes, which we discuss in detail in the supplementary.

6 Conclusions

In this work, we introduced the first 4D generative model that synthesizes realistic 3D-aware videos, supervised only from a set of unstructured 2D videos. Our proposed model combines the benefits of video and 3D generative models to enable new visual effects that involve spatio-temporal renderings, while at the same time maintaining the visual fidelity. The resulting latent space of rich, decomposable

motion and 3D content sets up the foundation to exciting new avenue of research towards interactive content generation and editing that requires knowledge of underlying 3D structures and motion priors.

Acknowledgements This project was supported in part by ARL grant W911NF-21-2-0104, a Vannevar Bush Faculty Fellowship, a gift from the Adobe Corporation, a PECASE by the ARO, NSF award 1839974, Stanford HAI, and a Samsung GRO. Despoina Paschalidou was supported by the Swiss National Science Foundation under grant number P500PT_206946.

Appendix

A Video Results

We provide additional qualitative results on the FaceForensics [83], MEAD [108], TaiChi [91], and SkyTimelapse [113] datasets on our project page <https://sherwinbahmani.github.io/3dvidgen>. In particular, we show the generated videos for all datasets from various camera viewpoints in order to showcase the ability of our model to learn a distribution of 3D-aware videos, which we highly encourage readers to view.

Specifically, for the case of FaceForensics, we show generated videos with a forward-facing camera (see Ours with Forward-facing Camera), with a camera that rotates along the yaw-axis (see Ours with Rotating Camera) and with a forward-facing camera that moves away from the depicted individual, thus creating a zoom-out effect, (see Ours with Forward-facing Camera and Zoom Effect). Moreover, we also provide generated videos using a variant of our model that uses a pre-trained generator on FFHQ [44], as discussed in the main submission and in Sec. D. This variant of our model allows a wider range of viewpoint control than our original model. Particularly, for this variant of our model, we also show examples of generated videos, while we rotate the camera along both yaw and pitch axes, where the fine-tuned model generates realistically looking videos. In addition, we show "Motion and Content Decomposition" examples, where we show the ability of our approach to control shape and motion separately; i.e., we can create videos illustrating the same human performing different motions, and vice versa. We also provide example videos of prior work including MoCoGAN-HD [102], DIGAN [116] and StyleGAN-V [95]. We note that our generated videos are of comparable quality against those of the state-of-the-art video generation methods [116, 95], while at the same time permitting control on the camera viewpoint, e.g., zoom-out to reveal new content or rotate the camera around, which is not possible for the latest 2D video methods.

Similarly, we also showcase examples of our generated videos on the MEAD [108] dataset using a similar setup. We observe that in comparison to StyleGAN-V [95] our generations have significantly fewer visual artifacts (the faces of [95] appear uncanny), while at the same time our generated videos from different camera viewpoints (see Ours with Different Camera Positions) are consistently plausible.

We also show examples of generated videos on the TaiChi [91] dataset using a similar setup. In addition, we also consider two more setups, where we rotate the camera along the yaw-axis while having a static human (see Ours with Rotating Camera and Static Motion) and a moving human (see Ours with Rotating Camera and Dynamic Motion). Also for these scenarios, the quality of our generated videos are comparable to that of DIGAN [116] that does not allow viewpoint control.

Finally, we show samples for the SkyTimelapse [113] dataset. The dataset is in contrast with the other three datasets, as its videos often contain multiple objects or entities. We provide videos rendered from a fixed camera, and a rotating camera along the yaw-axis with and without scene dynamics (Ours with Rotating Camera along First Axis and Static Motion, and Ours with Rotating Camera along First Axis and Dynamic Motion). Similarly, we rotate the camera along the pitch-axis with and without scene motions (Ours with Rotating Camera along Second Axis and Static Motion, and Ours with Rotating Camera along Second Axis and Dynamic Motion). Note that we only model rotation of a camera located at the origin. A careful modeling of camera distribution for such a large-scale scene dataset is out of scope of this work, and thus we omit an in-depth analysis.

B Implementation Details

B.1 Architecture and Training Details

The 3D content code, motion code and style vector dimensions are all set to 512. Our motion generator (see Fig. 2) is implemented as an MLP with three fully connected (FC) layers and Leaky ReLU activations. The time step is repeated across the channel dimension and multiplied with the output of the first fully connected layer of the motion generator. We set the motion code and hidden dimension of the motion generator to 512, while the output dimension is 128. The output of the motion generator is then added to the output of the first FG NeRF Block, which also is a 128-dimensional representation.

Our foreground and background NeRF are modeled as MLPs (with Leaky ReLU activations) with 8 and 4 FC layers that each contain 128 and 64 hidden units, respectively. We use 10 frequency bands to map the positional input of the foreground background NeRF to the fourier features [63]. We do not apply positional encoding to the time input. We follow the implementation of StyleNeRF [28] for the 2D ray aggregation and upsampling block (see Fig. 2) and the volume rendering process. Both the image and video discriminator follow the architecture of StyleGAN2 [45] with hidden dimensions of 512, and the input channels being 3 and 7, respectively. We apply the Differentiable Augmentation technique [122] with all augmentations except CutOut, to prevent the discriminators from overfitting to the relatively small video datasets. In contrast to StyleNeRF [28], we do not use progressive-growing training [42] but directly train on the final image resolution, as we did not observe any change in visual quality.

For both the generator and discriminator, we use the Adam optimizer [46] with a learning rate of 0.0025, $\beta_1 = 0$, $\beta_2 = 0.99$ and $\epsilon = 10^{-8}$. We follow the setup of StyleGAN2 [45] to use 8 fully connected layer content mapping network and apply $100\times$ lower learning rate compared to that of the main generator layers. For our objective function (Eq. 7), we set $\lambda_1 = 0.5$ and $\lambda_2 = 0.2$. We use 16 samples for the NeRF path regularization [28].

B.2 Virtual Camera Setup

For the three main datasets we set the virtual camera on the surface of unit sphere, and parameterize the camera viewpoint distribution with pitch and yaw angles. The standard deviation for pitch sampling is 0.15 for all three datasets. For yaw sampling the standard deviation is 0.3, 0.3, and 0.8 for FaceForensics, MEAD, TaiChi. The field-of-view of the camera is set to be 18 degrees.

For the SkyTimelapse dataset we do not sample on a sphere, but place the camera at the origin and make the camera look outwards. We uniformly sample a point on a hemisphere and set the camera to look towards the direction. The field-of-view is set to be 80 degrees. Note that this setup only models rotation of the camera. We leave a more complicated camera sampling method as future work.

C Experiment Details

C.1 Evaluations

We used the code and evaluation protocol of StyleGAN-V [95] for computing FVD [105] and FID [33]. The FVD protocol requires 2048 16-frame videos, while the FID score uses 50K images. For MEAD dataset [108], we re-trained StyleGAN-V [95] using their official code as the authors only provided results on the front view videos of MEAD at 1024^2 resolution. We randomly choose 10,000 videos across all viewpoints, including non-frontal views and follow the identical training setup provided by [95] to process 25,000K images with batch size 64. For TaiChi dataset, we use the officially provided checkpoint of DIGAN [116] to evaluate their model with the new FVD protocol [95]. For FaceForensics dataset, we use the reported numbers provided by the StyleGAN-V [95] authors for all models in Table 1, except for StyleNeRF [28] and our model, which we train from scratch.

We train our model and StyleNeRF using 4 NVIDIA V100 GPUs. For our approach we train for a maximum of 3,000K images, which takes two days at 256^2 resolution. For StyleNeRF we abort the training after 15,000K images due to the FID diverging after 11,400K images. It is generally true that 2D models like StyleGAN-V [95] have a significantly faster throughput, as there is no costly

Dataset	FVD Relative Standard Deviation
FaceForensics	2.62%
TaiChi	1.65%
MEAD	2.17%

Table 3: Relative standard deviation for the FVD metric on FaceForensics, TaiChi, and MEAD datasets, computed as percentage of standard deviation with respect to the mean.



Figure 7: Comparing the range of pitch control. We show that our 4D model trained solely on the FaceForensics [83] dataset (top row) has a narrow range of pitch where high quality renderings can be produced, likely due to the lack of diverse training views. Note that the upper and bottom parts of the head becomes unnaturally large at both extremes. Fine-tuning a model pre-trained on FFHQ [44] image dataset (bottom row), which features more diverse view angles, results in a wider range of views that generate plausible images.

volume rendering. However, we observe that our 4D model converges at much lower iterations, already converging after 2,500K processed images, while some of the 2D video models such as VideoGPT [114] does not converge even at 25,000K processed images. We hypothesize that the extraordinary fast convergence of our model is due to the explicit disentanglement of 3D content, camera viewpoints, and motions.

C.2 Reproducibility

For computing the FVD, we follow the protocol of StyleGAN-V [95], which aims to reduce the score variations significantly compared to the original protocol [105]. Nevertheless, in Table 3 we report the relative standard deviations after evaluating our three main dataset results for 10 rounds with the FVD protocol [95]. We observe that the standard deviation is rather small across all three datasets, as reported in the extensive analysis of [95].

D Training on Image and Video Datasets

In this section we discuss the use of an auxiliary 2D image dataset for training our 4D GANs, as described in Sec. 3.2 in the main paper. As motivated in the main paper, the lack of diversity of the provided videos could diminish the 3D accuracy of 4D GANs. In fact, we observe that the model trained only on the FaceForensics dataset [83] exhibits narrow range of camera angles that generates view-consistent renderings.

As described in the main paper, we explored two options to leverage an image dataset to complement the video dataset: (i) pre-training on the image dataset, and (ii) simultaneously training both on image and video datasets. For both options, we follow the training setup of StyleNeRF [28] on computing and backpropagating the image losses.

The model pre-trained on the FFHQ image dataset and fine-tuned on the video dataset generates high quality, 3D-aware renderings, as can be seen on the supplementary videos. We generally observe sharper and higher quality renderings compared to our default model. Moreover, we notice that the range of allowed view angles increases, which is most obvious for the pitch (or elevation) angles, as

described in Fig. 7. We note, however, that the colors seem less vivid compared to the pure-video model.

For the case of simultaneous image and video training, the resulting model fails to output view-consistent videos. We hypothesize that training the generators to fit two different data distributions does not lead to consistent 4D models.

E Limitations & Discussions (continued)

As mentioned in the main paper, we inherit the features of existing 3D-aware GANs that typically work the best when there is a single target object at the center of the scenes, e.g., human faces. A possible way of modeling multi-object scenes is to add in compositionality to scene distribution modeling (as in [69, 36]). Another factor that limits the modeling of larger and more complex scene is sampling of virtual cameras. Training of GANs involves approximating the input data distribution with the generators. For the case of 3D GANs, image generation requires sampling virtual viewpoints from a plausible viewpoint distribution, which could be designed manually for single-object scenes with outside-inward looking cameras. However, for larger scenes, obtaining or designing the plausible viewpoint distribution becomes challenging, due to lack of correspondences across scenes and high structural variability. An interesting future direction would be to model the camera viewpoint distribution using neural networks.

We find that there is noticeable dearth of high quality video data suitable for 3D-video GAN training. For instance, FaceForensics dataset [83] contains disproportionately many number of frontfacing videos, making it challenging to extract 3D structures. MEAD dataset [108], on the other hands, provides discrete set of fixed views that makes it difficult to predict viewpoints in between the provided view angles. The recent Talking Head dataset [110] provides 500 thousand high quality video clips of talking heads, which is potentially a promising dataset for future 4D GAN research. However, our close inspection of the dataset revealed that a significant portion of the videos are involved with absence of heads, occlusions, and other noises that need to be cleaned up, likely due to their reliance on off-the-shelf face detectors.

While our 4D GAN compares competitively in terms of training time until convergence, we note that the volume rendering process or our approach leaves huge memory footprints. In fact, training of our model consumes "2.4 GB / batch size," while the 2D video method of StyleGAN-V [95] only consumes "0.8 GB / batch size." This relatively high memory consumption prevents us from using larger models with the highest generation qualities. We leave exploration of more efficient implicit representations, such as tri-plane representations [9], as future work.

F Potential Negative Societal Impacts

While we see our work as an important step towards controllable video generation, we realize that it also bares the risk of being used for creating misleading or unethical content such as generating videos, where one person is replaced by another individual (DeepFake). Therefore, we strongly believe that the research community should seek to develop methods that can successfully identify real from synthetically generated content. While automating the generation process is an important step towards developing autonomous agents, we believe that we should also be equipped with appropriate tools that would prevent the use of generated videos for unethical purposes. Similar to prior work [116], our work can also be used towards this goal. In particular, we can utilize our discriminator for detecting real from fake content, since it was trained exactly on this task.

References

- [1] Dinesh Acharya, Zhiwu Huang, Danda Pani Paudel, and Luc Van Gool. Towards high resolution video generation with progressive growing of sliced wasserstein gans. *arXiv.org*, abs/1810.02419, 2018.
- [2] Abhishek Aich, Akash Gupta, Rameswar Panda, Rakib Hyder, M. Salman Asif, and Amit K. Roy-Chowdhury. Non-adversarial video synthesis with learned priors. In *Proc. IEEE Conf. on Computer Vision and Pattern Recognition (CVPR)*, 2020.
- [3] Yazeed Alharbi and Peter Wonka. Disentangled image generation through structured noise injection. In *Proc. IEEE Conf. on Computer Vision and Pattern Recognition (CVPR)*, 2020.

- [4] Matan Atzmon, Niv Haim, Lior Yariv, Ofer Israelov, Haggai Maron, and Yaron Lipman. Controlling neural level sets. In *Advances in Neural Information Processing Systems (NeurIPS)*, 2019.
- [5] Jonathan T. Barron, Ben Mildenhall, Matthew Tancik, Peter Hedman, Ricardo Martin-Brualla, and Pratul P. Srinivasan. Mip-nerf: A multiscale representation for anti-aliasing neural radiance fields. In *Proc. of the IEEE International Conf. on Computer Vision (ICCV)*, 2021.
- [6] Alexander W. Bergman, Petr Kellnhofer, and Gordon Wetzstein. Fast training of neural lumigraph representations using meta learning. In *Advances in Neural Information Processing Systems (NeurIPS)*, 2021.
- [7] Andrew Brock, Jeff Donahue, and Karen Simonyan. Large scale GAN training for high fidelity natural image synthesis. In *Proc. of the International Conf. on Learning Representations (ICLR)*, 2019.
- [8] Rohan Chabra, Jan Eric Lenssen, Eddy Ilg, Tanner Schmidt, Julian Straub, Steven Lovegrove, and Richard A. Newcombe. Deep local shapes: Learning local sdf priors for detailed 3d reconstruction. In Andrea Vedaldi, Horst Bischof, Thomas Brox, and Jan-Michael Frahm, editors, *Proc. of the European Conf. on Computer Vision (ECCV)*, 2020.
- [9] Eric R Chan, Connor Z Lin, Matthew A Chan, Koki Nagano, Boxiao Pan, Shalini De Mello, Orazio Gallo, Leonidas Guibas, Jonathan Tremblay, Sameh Khamis, Tero Karras, and Gordon Wetzstein. Efficient geometry-aware 3d generative adversarial networks. In *Proc. IEEE Conf. on Computer Vision and Pattern Recognition (CVPR)*, 2022.
- [10] Eric R Chan, Marco Monteiro, Petr Kellnhofer, Jiajun Wu, and Gordon Wetzstein. Pi-gan: Periodic implicit generative adversarial networks for 3d-aware image synthesis. In *Proc. IEEE Conf. on Computer Vision and Pattern Recognition (CVPR)*, 2021.
- [11] Hao Chen, Bo He, Hanyu Wang, Yixuan Ren, Ser Nam Lim, and Abhinav Shrivastava. Nerv: Neural representations for videos. In *Advances in Neural Information Processing Systems (NeurIPS)*, 2021.
- [12] Jianchuan Chen, Ying Zhang, Di Kang, Xuefei Zhe, Linchao Bao, Xu Jia, and Huchuan Lu. Animatable neural radiance fields from monocular rgb videos. *arXiv.org*, abs/2012.05903, 2021.
- [13] Xi Chen, Yan Duan, Rein Houthoofd, John Schulman, Ilya Sutskever, and Pieter Abbeel. Infogan: Interpretable representation learning by information maximizing generative adversarial nets. In *Advances in Neural Information Processing Systems (NIPS)*, 2016.
- [14] Zhiqin Chen and Hao Zhang. Learning implicit fields for generative shape modeling. *Proc. IEEE Conf. on Computer Vision and Pattern Recognition (CVPR)*, 2019.
- [15] Julian Chibane, Thiemo Alldieck, and Gerard Pons-Moll. Implicit functions in feature space for 3d shape reconstruction and completion. In *Proc. IEEE Conf. on Computer Vision and Pattern Recognition (CVPR)*, 2020.
- [16] Yunje Choi, Min-Je Choi, Munyoung Kim, Jung-Woo Ha, Sunghun Kim, and Jaegul Choo. Stargan: Unified generative adversarial networks for multi-domain image-to-image translation. In *Proc. IEEE Conf. on Computer Vision and Pattern Recognition (CVPR)*, 2018.
- [17] Aidan Clark, Jeff Donahue, and Karen Simonyan. Adversarial video generation on complex datasets. *arXiv.org*, abs/1907.06571, 2019.
- [18] Yu Deng, Jiaolong Yang, Jianfeng Xiang, and Xin Tong. Gram: Generative radiance manifolds for 3d-aware image generation. In *Proc. IEEE Conf. on Computer Vision and Pattern Recognition (CVPR)*, 2022.
- [19] Terrance DeVries, Miguel Ángel Bautista, Nitish Srivastava, Graham W. Taylor, and Joshua M. Susskind. Unconstrained scene generation with locally conditioned radiance fields. In *Proc. of the IEEE International Conf. on Computer Vision (ICCV)*, 2021.
- [20] Gereon Fox, Ayush Tewari, Mohamed Elgharib, and Christian Theobalt. Stylevideogan: A temporal generative model using a pretrained stylegan. In *Proc. of the British Machine Vision Conf. (BMVC)*, 2021.
- [21] Matheus Gadelha, Subhransu Maji, and Rui Wang. 3d shape induction from 2d views of multiple objects. In *Proc. of the International Conf. on 3D Vision (3DV)*, 2017.
- [22] Chen Gao, Ayush Saraf, Johannes Kopf, and Jia-Bin Huang. Dynamic view synthesis from dynamic monocular video. In *Proc. of the IEEE International Conf. on Computer Vision (ICCV)*, 2021.

- [23] Chen Gao, Yi-Chang Shih, Wei-Sheng Lai, Chia-Kai Liang, and Jia-Bin Huang. Portrait neural radiance fields from a single image. *arXiv.org*, abs/2012.05903, 2020.
- [24] Kyle Genova, Forrester Cole, Daniel Vlasic, Aaron Sarna, William T Freeman, and Thomas Funkhouser. Learning shape templates with structured implicit functions. In *Proc. of the IEEE International Conf. on Computer Vision (ICCV)*, 2019.
- [25] Ian J. Goodfellow, Jean Pouget-Abadie, Mehdi Mirza, Bing Xu, David Warde-Farley, Sherjil Ozair, Aaron C. Courville, and Yoshua Bengio. Generative adversarial nets. In *Advances in Neural Information Processing Systems (NIPS)*, 2014.
- [26] Cade Gordon and Natalie Parde. Latent neural differential equations for video generation. In *Advances in Neural Information Processing Systems (NeurIPS) Workshops*, 2020.
- [27] Amos Gropp, Lior Yariv, Niv Haim, Matan Atzmon, and Yaron Lipman. Implicit geometric regularization for learning shapes. In *Proc. of the International Conf. on Machine learning (ICML)*, 2020.
- [28] Jiatao Gu, Lingjie Liu, Peng Wang, and Christian Theobalt. Stylenerf: A style-based 3d-aware generator for high-resolution image synthesis. In *Proc. of the International Conf. on Learning Representations (ICLR)*, 2022.
- [29] Zekun Hao, Arun Mallya, Serge J. Belongie, and Ming-Yu Liu. Gancraft: Unsupervised 3d neural rendering of minecraft worlds. In *Proc. of the IEEE International Conf. on Computer Vision (ICCV)*, 2021.
- [30] Paul Henderson and Vittorio Ferrari. Learning single-image 3d reconstruction by generative modelling of shape, pose and shading. *International Journal of Computer Vision (IJCV)*, 2019.
- [31] Paul Henderson and Christoph H. Lampert. Unsupervised object-centric video generation and decomposition in 3d. In *Advances in Neural Information Processing Systems (NeurIPS)*, 2020.
- [32] Philipp Henzler, Niloy J Mitra, , and Tobias Ritschel. Escaping plato’s cave: 3d shape from adversarial rendering. In *Proc. of the IEEE International Conf. on Computer Vision (ICCV)*, 2019.
- [33] Martin Heusel, Hubert Ramsauer, Thomas Unterthiner, Bernhard Nessler, and Sepp Hochreiter. Gans trained by a two time-scale update rule converge to a local nash equilibrium. In *Advances in Neural Information Processing Systems (NIPS)*, 2017.
- [34] Aleksander Holynski, Brian L Curless, Steven M Seitz, and Richard Szeliski. Animating pictures with eulerian motion fields. In *Proc. IEEE Conf. on Computer Vision and Pattern Recognition (CVPR)*, 2021.
- [35] He Huang, Philip S. Yu, and Changhu Wang. An introduction to image synthesis with generative adversarial nets. *arXiv.org*, abs/1803.04469, 2018.
- [36] Drew A Hudson and Larry Zitnick. Generative adversarial transformers. In *Proc. of the International Conf. on Machine learning (ICML)*, 2021.
- [37] Sangeek Hyun, Jihwan Kim, and Jae-Pil Heo. Self-supervised video gans: Learning for appearance consistency and motion coherency. In *Proc. IEEE Conf. on Computer Vision and Pattern Recognition (CVPR)*, 2021.
- [38] Phillip Isola, Jun-Yan Zhu, Tinghui Zhou, and Alexei A. Efros. Image-to-image translation with conditional adversarial networks. In *Proc. IEEE Conf. on Computer Vision and Pattern Recognition (CVPR)*, 2017.
- [39] Chiyu Jiang, Avneesh Sud, Ameesh Makadia, Jingwei Huang, Matthias Nießner, and Thomas Funkhouser. Local implicit grid representations for 3d scenes. In *Proc. IEEE Conf. on Computer Vision and Pattern Recognition (CVPR)*, 2020.
- [40] Emmanuel Kahembwe and Subramanian Ramamoorthy. Lower dimensional kernels for video discriminators. *arXiv.org*, abs/1912.08860, 2019.
- [41] Nal Kalchbrenner, Aäron van den Oord, Karen Simonyan, Ivo Danihelka, Oriol Vinyals, Alex Graves, and Koray Kavukcuoglu. Video pixel networks. In *Proc. of the International Conf. on Machine learning (ICML)*, 2017.
- [42] Tero Karras, Timo Aila, Samuli Laine, and Jaakko Lehtinen. Progressive growing of gans for improved quality, stability, and variation. In *Proc. of the International Conf. on Learning Representations (ICLR)*, 2018.

- [43] Tero Karras, Miika Aittala, Samuli Laine, Erik Härkönen, Janne Hellsten, Jaakko Lehtinen, and Timo Aila. Alias-free generative adversarial networks. In *Advances in Neural Information Processing Systems (NeurIPS)*, 2021.
- [44] Tero Karras, Samuli Laine, and Timo Aila. A style-based generator architecture for generative adversarial networks. In *Proc. IEEE Conf. on Computer Vision and Pattern Recognition (CVPR)*, 2019.
- [45] Tero Karras, Samuli Laine, Miika Aittala, Janne Hellsten, Jaakko Lehtinen, and Timo Aila. Analyzing and improving the image quality of stylegan. In *Proc. IEEE Conf. on Computer Vision and Pattern Recognition (CVPR)*, 2020.
- [46] Diederik P Kingma and Jimmy Ba. Adam: A method for stochastic optimization. In *Proc. of the International Conf. on Learning Representations (ICLR)*, 2015.
- [47] Wonkwang Lee, Donggyun Kim, Seunghoon Hong, and Honglak Lee. High-fidelity synthesis with disentangled representation. In *Proc. of the European Conf. on Computer Vision (ECCV)*, 2020.
- [48] Zhengqi Li, Simon Niklaus, Noah Snavely, and Oliver Wang. Neural scene flow fields for space-time view synthesis of dynamic scenes. In *Proc. IEEE Conf. on Computer Vision and Pattern Recognition (CVPR)*, 2021.
- [49] Yiyi Liao, Katja Schwarz, Lars Mescheder, and Andreas Geiger. Towards unsupervised learning of generative models for 3d controllable image synthesis. In *Proc. IEEE Conf. on Computer Vision and Pattern Recognition (CVPR)*, 2020.
- [50] Chen-Hsuan Lin, Chaoyang Wang, and Simon Lucey. Sdf-srn: Learning signed distance 3d object reconstruction from static images. In *Advances in Neural Information Processing Systems (NeurIPS)*, 2020.
- [51] Connor Z. Lin, David B. Lindell, Eric Chan, and Gordon Wetzstein. 3d gan inversion for controllable portrait image animation. *arXiv.org*, abs/2203.13441, 2022.
- [52] David B Lindell, Dave Van Veen, Jeong Joon Park, and Gordon Wetzstein. Bacon: Band-limited coordinate networks for multiscale scene representation. In *Proc. IEEE Conf. on Computer Vision and Pattern Recognition (CVPR)*, 2022.
- [53] Huan Ling, Karsten Kreis, Daiqing Li, Seung Wook Kim, Antonio Torralba, and Sanja Fidler. Editgan: High-precision semantic image editing. In *Advances in Neural Information Processing Systems (NeurIPS)*, 2021.
- [54] Lingjie Liu, Jiatao Gu, Kyaw Zaw Lin, Tat-Seng Chua, and Christian Theobalt. Neural sparse voxel fields. In *Advances in Neural Information Processing Systems (NeurIPS)*, 2020.
- [55] Lingjie Liu, Marc Habermann, Viktor Rudnev, Kripasindhu Sarkar, Jiatao Gu, and Christian Theobalt. Neural actor: Neural free-view synthesis of human actors with pose control. In *ACM Trans. on Graphics*, 2021.
- [56] Stephen Lombardi, Tomas Simon, Jason Saragih, Gabriel Schwartz, Andreas Lehrmann, and Yaser Sheikh. Neural volumes: Learning dynamic renderable volumes from images. In *ACM Trans. on Graphics*, 2019.
- [57] Sebastian Lunz, Yingzhen Li, Andrew W. Fitzgibbon, and Nate Kushman. Inverse graphics gan: Learning to generate 3d shapes from unstructured 2d data. *arXiv.org*, abs/2002.12674, 2020.
- [58] Ricardo Martin-Brualla, Noha Radwan, Mehdi S. M. Sajjadi, Jonathan T. Barron, Alexey Dosovitskiy, and Daniel Duckworth. Nerf in the wild: Neural radiance fields for unconstrained photo collections. In *Proc. IEEE Conf. on Computer Vision and Pattern Recognition (CVPR)*, 2021.
- [59] Quan Meng, Anpei Chen, Haimin Luo, Minye Wu, Hao Su, Lan Xu, Xuming He, and Jingyi Yu. Gnerf: Gan-based neural radiance field without posed camera. In *Proc. of the IEEE International Conf. on Computer Vision (ICCV)*, 2021.
- [60] Lars Mescheder, Andreas Geiger, and Sebastian Nowozin. Which training methods for gans do actually converge? In *Proc. of the International Conf. on Machine learning (ICML)*, 2018.
- [61] Lars Mescheder, Michael Oechsle, Michael Niemeyer, Sebastian Nowozin, and Andreas Geiger. Occupancy networks: Learning 3d reconstruction in function space. In *Proc. IEEE Conf. on Computer Vision and Pattern Recognition (CVPR)*, 2019.

- [62] Mateusz Michalkiewicz, Jhony K Pontes, Dominic Jack, Mahsa Baktashmotlagh, and Anders Eriksson. Implicit surface representations as layers in neural networks. In *Proc. of the IEEE International Conf. on Computer Vision (ICCV)*, 2019.
- [63] Ben Mildenhall, Pratul P Srinivasan, Matthew Tancik, Jonathan T Barron, Ravi Ramamoorthi, and Ren Ng. Nerf: Representing scenes as neural radiance fields for view synthesis. In *Proc. of the European Conf. on Computer Vision (ECCV)*, 2020.
- [64] Andrés Muñoz, Mohammadreza Zolfaghari, Max Argus, and Thomas Brox. Temporal shift gan for large scale video generation. In *Proc. of the IEEE Winter Conference on Applications of Computer Vision (WACV)*, 2021.
- [65] Thu Nguyen-Phuoc, Chuan Li, Stephen Balaban, and Yong-Liang Yang. Rendernet: A deep convolutional network for differentiable rendering from 3d shapes. In *Advances in Neural Information Processing Systems (NIPS)*, 2018.
- [66] Thu Nguyen-Phuoc, Chuan Li, Lucas Theis, Christian Richardt, and Yong-Liang Yang. Hologan: Unsupervised learning of 3d representations from natural images. In *Proc. of the IEEE International Conf. on Computer Vision (ICCV)*, 2019.
- [67] Thu Nguyen-Phuoc, Christian Richardt, Long Mai, Yong-Liang Yang, and Niloy Mitra. Blockgan: Learning 3d object-aware scene representations from unlabelled images. In *Advances in Neural Information Processing Systems (NeurIPS)*, 2020.
- [68] Michael Niemeyer and Andreas Geiger. Campari: Camera-aware decomposed generative neural radiance fields. In *Proc. of the International Conf. on 3D Vision (3DV)*, 2021.
- [69] Michael Niemeyer and Andreas Geiger. Giraffe: Representing scenes as compositional generative neural feature fields. In *Proc. IEEE Conf. on Computer Vision and Pattern Recognition (CVPR)*, 2021.
- [70] Michael Niemeyer, Lars M. Mescheder, Michael Oechsle, and Andreas Geiger. Differentiable volumetric rendering: Learning implicit 3d representations without 3d supervision. In *Proc. IEEE Conf. on Computer Vision and Pattern Recognition (CVPR)*, 2020.
- [71] Michael Oechsle, Songyou Peng, and Andreas Geiger. Unisurf: Unifying neural implicit surfaces and radiance fields for multi-view reconstruction. In *Proc. of the IEEE International Conf. on Computer Vision (ICCV)*, 2021.
- [72] Roy Or-El, Xuan Luo, Mengyi Shan, Eli Shechtman, Jeong Joon Park, and Ira Kemelmacher-Shlizerman. Stylesdf: High-resolution 3d-consistent image and geometry generation. In *Proc. IEEE Conf. on Computer Vision and Pattern Recognition (CVPR)*, 2022.
- [73] Eunbyung Park, Jimei Yang, Ersin Yumer, Duygu Ceylan, and Alexander C. Berg. Transformation-grounded image generation network for novel 3d view synthesis. In *Proc. IEEE Conf. on Computer Vision and Pattern Recognition (CVPR)*, 2017.
- [74] Jeong Joon Park, Peter Florence, Julian Straub, Richard Newcombe, and Steven Lovegrove. Deep sdf: Learning continuous signed distance functions for shape representation. In *Proc. IEEE Conf. on Computer Vision and Pattern Recognition (CVPR)*, 2019.
- [75] Keunhong Park, Utkarsh Sinha, Jonathan T. Barron, Sofien Bouaziz, Dan B. Goldman, Steven M. Seitz, and Ricardo Martin-Brualla. Nerfies: Deformable neural radiance fields. In *Proc. of the IEEE International Conf. on Computer Vision (ICCV)*, 2021.
- [76] Keunhong Park, Utkarsh Sinha, Peter Hedman, Jonathan T. Barron, Sofien Bouaziz, Dan B. Goldman, Ricardo Martin-Brualla, and Steven M. Seitz. Hypernerf: a higher-dimensional representation for topologically varying neural radiance fields. *ACM Trans. on Graphics*, 2021.
- [77] Songyou Peng, Michael Niemeyer, Lars Mescheder, Marc Pollefeys, and Andreas Geiger. Convolutional occupancy networks. In *Proc. of the European Conf. on Computer Vision (ECCV)*, 2020.
- [78] Martin Píala and Ronald Clark. Terminerf: Ray termination prediction for efficient neural rendering. In *Proc. of the International Conf. on 3D Vision (3DV)*, 2021.
- [79] Albert Pumarola, Enric Corona, Gerard Pons-Moll, and Francesc Moreno-Noguer. D-nerf: Neural radiance fields for dynamic scenes. In *Proc. IEEE Conf. on Computer Vision and Pattern Recognition (CVPR)*, 2021.

- [80] Ruslan Rakhimov, Denis Volkhonskiy, Alexey Artemov, Denis Zorin, and Evgeny Burnaev. Latent video transformer. *arXiv.org*, abs/2006.10704, 2020.
- [81] Scott E. Reed, Kihyuk Sohn, Yuting Zhang, and Honglak Lee. Learning to disentangle factors of variation with manifold interaction. In *Proc. of the International Conf. on Machine learning (ICML)*, 2014.
- [82] Yurui Ren, Ge Li, Yuanqi Chen, Thomas H Li, and Shan Liu. Pirenderer: Controllable portrait image generation via semantic neural rendering. In *Proc. of the IEEE International Conf. on Computer Vision (ICCV)*, 2021.
- [83] Andreas Rössler, Davide Cozzolino, Luisa Verdoliva, Christian Riess, Justus Thies, and Matthias Nießner. Faceforensics++: Learning to detect manipulated facial images. In *Proc. of the IEEE International Conf. on Computer Vision (ICCV)*, 2019.
- [84] Masaki Saito, Eiichi Matsumoto, and Shunta Saito. Temporal generative adversarial nets with singular value clipping. In *Proc. of the IEEE International Conf. on Computer Vision (ICCV)*, 2017.
- [85] Masaki Saito, Shunta Saito, Masanori Koyama, and Sosuke Kobayashi. Train sparsely, generate densely: Memory-efficient unsupervised training of high-resolution temporal GAN. *International Journal of Computer Vision (IJCV)*, 2020.
- [86] Shunsuke Saito, Zeng Huang, Ryota Natsume, Shigeo Morishima, Angjoo Kanazawa, and Hao Li. Pifu: Pixel-aligned implicit function for high-resolution clothed human digitization. In *Proc. of the IEEE International Conf. on Computer Vision (ICCV)*, 2019.
- [87] Mehdi S. M. Sajjadi, Henning Meyer, Etienne Pot, Urs Bergmann, Klaus Greff, Noha Radwan, Suhani Vora, Mario Lucic, Daniel Duckworth, Alexey Dosovitskiy, Jakob Uszkoreit, Thomas A. Funkhouser, and Andrea Tagliasacchi. Scene representation transformer: Geometry-free novel view synthesis through set-latent scene representations. In *Proc. IEEE Conf. on Computer Vision and Pattern Recognition (CVPR)*, 2022.
- [88] Katja Schwarz, Yiyi Liao, Michael Niemeyer, and Andreas Geiger. Graf: Generative radiance fields for 3d-aware image synthesis. In *Advances in Neural Information Processing Systems (NeurIPS)*, 2020.
- [89] Yujun Shen, Jinjin Gu, Xiaoou Tang, and Bolei Zhou. Interpreting the latent space of gans for semantic face editing. In *Proc. IEEE Conf. on Computer Vision and Pattern Recognition (CVPR)*, 2020.
- [90] Alon Shoshan, Nadav Bhonker, Igor Kviatkovsky, and Gerard Medioni. Gan-control: Explicitly controllable gans. In *Proc. of the IEEE International Conf. on Computer Vision (ICCV)*, 2021.
- [91] Aliaksandr Siarohin, Stéphane Lathuilière, Sergey Tulyakov, Elisa Ricci, and Nicu Sebe. First order motion model for image animation. In *Advances in Neural Information Processing Systems (NeurIPS)*, 2019.
- [92] Vincent Sitzmann, Julien N. P. Martel, Alexander W. Bergman, David B. Lindell, and Gordon Wetzstein. Implicit neural representations with periodic activation functions. In *Advances in Neural Information Processing Systems (NeurIPS)*, 2020.
- [93] Vincent Sitzmann, Michael Zollhöfer, and Gordon Wetzstein. Scene representation networks: Continuous 3d-structure-aware neural scene representations. In *Advances in Neural Information Processing Systems (NeurIPS)*, 2019.
- [94] Ivan Skorokhodov, Savva Ignatyev, and Mohamed Elhoseiny. Adversarial generation of continuous images. In *Proc. IEEE Conf. on Computer Vision and Pattern Recognition (CVPR)*, 2021.
- [95] Ivan Skorokhodov, Sergey Tulyakov, and Mohamed Elhoseiny. Stylegan-v: A continuous video generator with the price, image quality and perks of stylegan2. In *Proc. IEEE Conf. on Computer Vision and Pattern Recognition (CVPR)*, 2022.
- [96] Pratul P. Srinivasan, Boyang Deng, Xiuming Zhang, Matthew Tancik, Ben Mildenhall, and Jonathan T. Barron. Nerv: Neural reflectance and visibility fields for relighting and view synthesis. In *Proc. IEEE Conf. on Computer Vision and Pattern Recognition (CVPR)*, 2021.
- [97] Hao Tang, Dan Xu, Nicu Sebe, Yanzhi Wang, Jason J Corso, and Yan Yan. Multi-channel attention selection gan with cascaded semantic guidance for cross-view image translation. In *Proc. IEEE Conf. on Computer Vision and Pattern Recognition (CVPR)*, 2019.
- [98] Hao Tang, Dan Xu, Yan Yan, Philip HS Torr, and Nicu Sebe. Local class-specific and global image-level generative adversarial networks for semantic-guided scene generation. In *Proc. IEEE Conf. on Computer Vision and Pattern Recognition (CVPR)*, 2020.

- [99] Ayush Tewari, Mohamed Elgharib, Florian Bernard, Hans-Peter Seidel, Patrick Pérez, Michael Zollhöfer, and Christian Theobalt. Pie: Portrait image embedding for semantic control. In *ACM Trans. on Graphics*, 2020.
- [100] Ayush Tewari, Mohamed Elgharib, Gaurav Bharaj, Florian Bernard, Hans-Peter Seidel, Patrick Pérez, Michael Zollhofer, and Christian Theobalt. Stylerig: Rigging stylegan for 3d control over portrait images. In *Proc. IEEE Conf. on Computer Vision and Pattern Recognition (CVPR)*, 2020.
- [101] Ayush Tewari, Justus Thies, Ben Mildenhall, Pratul P. Srinivasan, Edgar Tretschk, Yifan Wang, Christoph Lassner, Vincent Sitzmann, Ricardo Martin-Brualla, Stephen Lombardi, Tomas Simon, Christian Theobalt, Matthias Nießner, Jonathan T. Barron, Gordon Wetzstein, Michael Zollhöfer, and Vladislav Golyanik. Advances in neural rendering. *arXiv.org*, abs/2111.05849, 2021.
- [102] Yu Tian, Jian Ren, Menglei Chai, Kyle Olszewski, Xi Peng, Dimitris N. Metaxas, and Sergey Tulyakov. A good image generator is what you need for high-resolution video synthesis. In *Proc. of the International Conf. on Learning Representations (ICLR)*, 2021.
- [103] Edgar Tretschk, Ayush Tewari, Vladislav Golyanik, Michael Zollhöfer, Christoph Lassner, and Christian Theobalt. Non-rigid neural radiance fields: Reconstruction and novel view synthesis of a dynamic scene from monocular video. In *Proc. of the IEEE International Conf. on Computer Vision (ICCV)*, 2021.
- [104] Sergey Tulyakov, Ming-Yu Liu, Xiaodong Yang, and Jan Kautz. Mocogan: Decomposing motion and content for video generation. In *Proc. IEEE Conf. on Computer Vision and Pattern Recognition (CVPR)*, 2018.
- [105] Thomas Unterthiner, Sjoerd van Steenkiste, Karol Kurach, Raphael Marinier, Marcin Michalski, and Sylvain Gelly. Towards accurate generative models of video: A new metric & challenges. *arXiv.org*, abs/1812.01717, 2018.
- [106] Jacob Walker, Ali Razavi, and Aäron van den Oord. Predicting video with VQVAE. *arXiv.org*, abs/2103.01950, 2021.
- [107] Binxu Wang and Carlos R. Ponce. A geometric analysis of deep generative image models and its applications. In *Proc. of the International Conf. on Learning Representations (ICLR)*, 2021.
- [108] Kaisiyuan Wang, Qianyi Wu, Linsen Song, Zhuoqian Yang, Wayne Wu, Chen Qian, Ran He, Yu Qiao, and Chen Change Loy. Mead: A large-scale audio-visual dataset for emotional talking-face generation. In *Proc. of the European Conf. on Computer Vision (ECCV)*, 2020.
- [109] Ting-Chun Wang, Ming-Yu Liu, Jun-Yan Zhu, Andrew Tao, Jan Kautz, and Bryan Catanzaro. High-resolution image synthesis and semantic manipulation with conditional gans. In *Proc. IEEE Conf. on Computer Vision and Pattern Recognition (CVPR)*, 2018.
- [110] Ting-Chun Wang, Arun Mallya, and Ming-Yu Liu. One-shot free-view neural talking-head synthesis for video conferencing. In *Proc. IEEE Conf. on Computer Vision and Pattern Recognition (CVPR)*, 2021.
- [111] Dirk Weissenborn, Oscar Täckström, and Jakob Uszkoreit. Scaling autoregressive video models. In *Proc. of the International Conf. on Learning Representations (ICLR)*, 2020.
- [112] Wenqi Xian, Jia-Bin Huang, Johannes Kopf, and Changil Kim. Space-time neural irradiance fields for free-viewpoint video. In *Proc. IEEE Conf. on Computer Vision and Pattern Recognition (CVPR)*, 2021.
- [113] Wei Xiong, Wenhan Luo, Lin Ma, Wei Liu, and Jiebo Luo. Learning to generate time-lapse videos using multi-stage dynamic generative adversarial networks. In *Proc. IEEE Conf. on Computer Vision and Pattern Recognition (CVPR)*, 2018.
- [114] Wilson Yan, Yunzhi Zhang, Pieter Abbeel, and Aravind Srinivas. Videogpt: Video generation using VQ-VAE and transformers. *arXiv.org*, abs/2104.10157, 2021.
- [115] Lior Yariv, Yoni Kasten, Dror Moran, Meirav Galun, Matan Atzmon, Ronen Basri, and Yaron Lipman. Multiview neural surface reconstruction by disentangling geometry and appearance. In *Advances in Neural Information Processing Systems (NeurIPS)*, 2020.
- [116] Sihyun Yu, Jihoon Tack, Sangwoo Mo, Hyunsu Kim, Junho Kim, Jung-Woo Ha, and Jinwoo Shin. Generating videos with dynamics-aware implicit generative adversarial networks. In *Proc. of the International Conf. on Learning Representations (ICLR)*, 2022.
- [117] Wentao Yuan, Zhaoyang Lv, Tanner Schmidt, and Steven Lovegrove. Star: Self-supervised tracking and reconstruction of rigid objects in motion with neural rendering. In *Proc. IEEE Conf. on Computer Vision and Pattern Recognition (CVPR)*, 2021.

- [118] Vladyslav Yushchenko, Nikita Araslanov, and Stefan Roth. Markov decision process for video generation. In *Proc. of the IEEE International Conf. on Computer Vision (ICCV) Workshops*, 2019.
- [119] Jiakai Zhang, Xinhang Liu, Xinyi Ye, Fuqiang Zhao, Yanshun Zhang, Minye Wu, Yingliang Zhang, Lan Xu, and Jingyi Yu. Editable free-viewpoint video using a layered neural representation. *ACM Trans. on Graphics*, 2021.
- [120] Kai Zhang, Gernot Riegler, Noah Snaveley, and Vladlen Koltun. Nerf++: Analyzing and improving neural radiance fields. *arXiv.org*, abs/2010.07492, 2020.
- [121] Bo Zhao, Bo Chang, Zequn Jie, and Leonid Sigal. Modular generative adversarial networks. In *Proc. of the European Conf. on Computer Vision (ECCV)*, 2018.
- [122] Shengyu Zhao, Zhijian Liu, Ji Lin, Jun-Yan Zhu, and Song Han. Differentiable augmentation for data-efficient gan training. In *Advances in Neural Information Processing Systems (NeurIPS)*, 2020.
- [123] Peng Zhou, Lingxi Xie, Bingbing Ni, and Qi Tian. Cips-3d: A 3d-aware generator of gans based on conditionally-independent pixel synthesis. *arXiv.org*, abs/2110.09788, 2021.
- [124] Jun-Yan Zhu, Taesung Park, Phillip Isola, and Alexei A. Efros. Unpaired image-to-image translation using cycle-consistent adversarial networks. In *Proc. of the IEEE International Conf. on Computer Vision (ICCV)*, 2017.